This is the author's peer reviewed, accepted manuscript. However, the online version of record will be different from this version once it has been copyedited and typeset. PLEASE OTE THIS ARTICLE AS DOI: 10.1063/5.0230223

In-plane Orientational Motions of the Functional Groups of Molecules at the Air/Water Interface by Time-Resolved Vibrational Sum Frequency Generation

Zhi-Chao Huang-Fu[#], Tong Zhang[#], Jesse B. Brown, Yuqin Qian, Haley Fisher, Yi Rao*

Department of Chemistry and Biochemistry, Utah State University, Logan, UT 84322, United States *Corresponding author: yi.rao@usu.edu

Abstract

The movements of molecules at interfaces and surfaces are restricted by their asymmetric environments, leading to anisotropic orientational motions. In this work, in-plane orientational motions of the -C=0 and $-CF_3$ groups of coumarin 153 (C153) at the air/water interface were measured using time-resolved vibrational sum frequency generation (TR-VSFG). The in-plane orientational time constants of the -C=0 and $-CF_3$ groups of C153 are found to be 41.5 \pm 8.2 ps and 36.0 \pm 4.5 ps. These values are over five-times faster than that of 198 \pm 15 ps for the permanent dipole of the whole C153 molecule at the interface, which may indicate that the two groups experience different interfacial friction in the plane. These differences could also be the result of the permanent dipole of C153 being almost five times those of the -C=0 and $-CF_3$ groups. The difference in orientational motions reveals the microscopic heterogeneous environment that molecules experience at the interface. While the interfacial dynamics of the two functional groups are similar, our TR-SFG experiments allowed the quantification of the in-plane dynamics of individual functional groups for the first time. Our experimental findings about the interfacial molecular motion have implications to molecular rotations, energy transfer, and charge transfer at materials interfaces, photocatalysis interfaces, and biological cell/membrane aqueous interfaces.

Introduction

The air/water interface, with its unique properties, is of special interest due to its relevance to our daily life, health, industry, and atmosphere. The asymmetric environment at the interface presents unique chemical and physical properties for molecular adsorbates. Due to the change of solvent properties at the interface and the inherent anisotropy of that environment, molecular interactions and motions at interfaces are anticipated to differ from those in bulk liquid. Therefore, the motions of a solute molecule at the air/water interface would be restricted by the asymmetric environment, leading to anisotropic orientational motions therein, *i.e.* the dynamics of rotation in the interfacial plane could differ from the out-of-plane orientational motions. The second solution is the interfacial plane could differ from the out-of-plane orientational motions.

Unlike the isotropic rotational motions of solutes in bulk water, the asymmetric potential energy at the interface restricts the rotational motions of adsorbed solutes. Interfacial molecules exhibit structure-based directionality at an air/aqueous interface, with one end of the molecule preferentially immersed in the condensed layer and the other largely found exposed to the vapor phase. ⁹⁻¹² This directionality is expected to be reflected in different interfacial molecular rotational motions, in and out of the interfacial plane. These anisotropic rotational motions are hypothesized to be sensitive to changes in the microscopic environment at density-gradient interfacial regions, since solvent ordering and its expression in interfacial friction strongly affect the timescales for

This is the author's peer reviewed, accepted manuscript. However, the online version of record will be different from this version once it has been copyedited and typeset. PLEASE OTE THIS ARTICLE AS DOI: 10.1063/5.0230223

molecular orientational relaxation. However, there has been no experimental evidence to date toward this hypothesis.

The surface specificity afforded by second harmonic generation (SHG) and sum frequency generation (SFG) spectroscopies provides a robust optical means to study the structure and dynamics of molecules present at interfacial regions. 10, 13-15 SHG and SFG have been used extensively to probe interfacial phenomena at gas-liquid, gas-solid, liquid-solid, and liquid-liquid interfaces in real time, and with molecular specificity. 14, 16-34 The utility afforded by the interfacial specificity of SHG, electronic SFG (ESFG), and vibrational SFG (VSFG) techniques can be further exploited by introducing an ultrafast pump pulse to excite the sample just prior to probing, resulting in time-resolved (TR) experiments, so-called TR-SHG and TR-ESFG/TR-VSFG. In these experiments, the pump pulse can excite the electronic (UV-vis wavelengths) or vibrational (IR wavelengths) resonances of a sample and then monitor the excited state over time. The first TR-SHG experiment was conducted by Sitzmann and Eisenthal,³⁵ where photoisomerization was observed in-situ for the first time at the air/water interface with a visible beam. Some years later, Sekiguchi et al. presented the first TR-ESFG using three nondegenerate waves to study ultrafast interfacial dynamics of dye molecules at the air/water interface. 36 While TR-ESFG has continued to advance over the years and has provided much important and exciting information about critical interfaces, we are primarily concerned with VSFG studies in the present work.

Early reports of TR-VSFG experiments primarily covered IR-pumped SFG-probed systems. 37-40 However, our primary focus here is the case with a UV or visible pump. One early report was made by Bonn et al., where incident pulses caused motion of adsorbed CO at Pt surface, as monitored with a VSFG probe. 41 In another interesting study, molecular-level heat transfer was investigated for long hydrocarbon chains by laser flash-heating their substrate and monitoring the terminal methyl groups with VSFG spectroscopy. 42 On the other hand, Rao et al. presented the first TR-VSFG experiments using a visible pump in electronic resonance with the analyte at the air/water interface⁴³. In this work, the molecular orientational dynamics of a chromophore at the air/water interface were investigated for the first time and exhibited ps time resolution. Later, they also used TR-VSFG to study solvation dynamics and determine solvation times of photoexcited chromophores at the air/water interface⁴⁴. As the technique progressed, the visible-pumped VSFG was extended to include heterodyne detection (TR-HD-VSFG), which investigated the dynamics at the air/water interface by separating the real and imaginary parts of the SFG response.⁴⁵ Furthermore, TR-VSFG has been used to obtain in-situ observations of electron transfer at semiconductor/organic film interfaces with excellent temporal resolution. 46 Most recently, visiblepump SFG methods have been further extended into two-dimensional (2D) techniques. In its debut, 2D electronic-vibrational SFG (2D-EVSFG) was achieved by mixing a phase-locked electronic pump pulse pair with VSFG of dye molecules at the air/water interface, showing the ability to uncover electronic-vibrational couplings therein, and monitor their progression over time along with generated locally excited modes.⁴⁷ Since then, 2D-EVSFG has been used to quantify the relative orientations of electronic and vibrational transition dipoles at the interface, monitor structural evolutions of excited states, 48 and to uncover vibronic coupling and solvent correlation dynamics at the air water interface in-situ.⁴⁹

The ability of SFG techniques to quantify molecular orientation at interfaces makes it an excellent choice to probe changes in orientation therein, such as rotation. For example, by exciting the water surface by a polarized IR pump pulse, VSFG was used to monitor the formed anisotropy

PLEASE OTE THIS ARTIOLE AS DOI: 10.1063/5.0230223

and subsequent equilibration at the air/water surface, finding that reordering occurred several times faster than in bulk water.⁵⁰ Due to the importance of rotational dynamics at the pure water surface, it has been investigated extensively.^{51, 52} VSFG has also shown that the crystal structure of a substrate can affect molecular rotations, where methyl groups turned an order of magnitude slower at the silicon surface than in the bulk.^{53, 54} In another study, it was found α-pinene molecules rotate with minimal restrictions on silica surface by conducting VSFG line-shape analyses and simulations due to the molecule's unique geometry.⁵⁵ However, TR-VSFG studies do offer a unique advantage over traditional, static SFG methods: the changes in the interfacial spectra upon excitation are more obvious than subtle changes in spectral line-shapes between different experiments, making their tracking more straightforward and eliminating potential errors that may come from complex data analysis. In other cases, Eisenthal et. al used TR-SHG to observe slower orientation times of coumarin 314 (C314) at the air/water interface relative to their bulk values.^{6, 8, 56} It was shown that both out-of- and in-plane interfacial relaxation times of the permanent dipole for C314 are significantly slower than that in bulk water. The interfacial relaxation time of C314 indicates that the rotational friction at the air/water interface is greater than that in bulk water.

In our previous study, we have presented the orientational motion of the –C=O group of C314with visible pump TR-SFG measurements.⁵ This previous research demonstrated the absolute orientational motions of a whole molecule for C314 by probing the out-of-plane orientational motions for the –C=O and –CF3 groups with TR-SFG. In this companion article, we shall concentrate on the in-plane orientational motions of the –C=O and –CF3 functional groups of coumarin 153 (C153) at the air/ water interface using TR-SFG. C314 and C153, aromatic chromophores, have similar structures where C153 has –C=O and –CF3 groups which point into the water and air phases, respectively. We chose to use C153 in this work due to the established knowledge base form previous experiments, interesting functional group configuration, and convenient resonant pumping frequency. Here, we focus on the in-plane dynamics of the functional groups and examine how they interact with solvent in the plane of the interface and how those interactions correlate with overall molecular dynamics.

PLEASE OTE THIS ARTICLE AS DOI: 10.1063/5.0230223

AIP AIP Publishing

(A) Z 60 pamp ω_{vis} (B) (C) X-polarized f-polarized excitation excitation

Figure 1. (A) Schematic setup of time-resolved vibrational sum frequency generation and the definition of a dipole at the air/water interface; (B) & (C) change in interfacial orientation distribution under X- and Y- polarized excitation along the surface normal, respectively. Dipoles highlighted in green have a greater probability of excitation.

Theoretical considerations

Before we can investigate orientational dynamics at the air/water interface, we shall define the system. First, to excite the sample, a linearly-polarized pump pulse is incident normal to the interfacial plane, along the Z-axis from above. Next, we treat the probed functional groups at the interface as a dipole oriented at an angle θ with respect to the Z- axis, and its projection onto the XY-plane has an angle ϕ with respect to the X-axis, as defined in Figure 1 (A). The static orientational distribution is depicted schematically in Figure 1 (B) and (C) as dipoles lying between two cones representing maximum and minimum θ . The linearly-polarized pump pulse photoexcites a subset of the interfacial equilibrium distribution of ground state molecules, thereby generating non-equilibrium orientational distributions in both out-of-plane and in-plane directions.

PLEASE OTE THIS ARTICLE AS DOI: 10.1063/5.0230223

Since the SFG signal is sensitive to a change in orientational distribution at the interface, it responds to both out-of-plane and in-plane motions which bring the ground and excited state molecules to their equilibrium orientations. As such, dipoles oriented along the *X*- or *Y*-axes are preferentially excited by probe pulses oriented along those respective directions, as schematically shown in Figure 1 (B) and (C). Therefore, both excitations from the *X*- or *Y*-polarized pump break the isotropic symmetry of the in-plane orientational distribution; and monitoring their changes over time relative to each other can outline the movements of the interfacial molecules. When pumped by a circularly-polarized laser along the surface normal, the symmetry of orientational distribution in the surface plane is not affected, whereas the symmetry of out-of-plane

When pumped by a circularly-polarized laser along the surface normal, the symmetry of orientational distribution in the surface plane is not affected, whereas the symmetry of out-of-plane orientational distribution is broken. When pumped by a linearly-polarized pulse along the surface normal, both out-of-plane and in-plane orientational distributions are broken in symmetry. Therefore, polarized SFG intensities respond differently to the circularly- and linearly-polarized excitations. To understand how time-dependent SFG intensities for a vibrational mode are related to in-plane orientational dynamics, we shall consider how the static and time-dependent SFG for a vibrational mode are affected by two different linearly-polarized excitations.

At equilibrium, when a symmetric stretching vibrational mode with $C_{\infty V}$ symmetry, like a – C=O group, and a symmetric stretching vibrational mode with C_{3V} symmetry, such as a –CF₃, group are considered, there are three non-vanishing hyperpolarizabilities $\alpha_{zzz}^{(2)} = r * \alpha_{xxz}^{(2)} = r * \alpha_{yyz}^{(2)}$, where r is the Raman ratio of the transverse polarizability and the longitudinal polarizability of the bond, and the subscripts in $\alpha_{ijk}^{(2)}$ refer to the local molecular coordinates. Thus, the seven interfacial second order susceptibilities, $\chi_{IJK}^{(2)}$, are related to the three molecular hyperpolarizabilities by spatial orientational averages of the orientational distributions: 31,60

$$\begin{split} \chi_{XXZ}^{(2)} &= N\alpha_{zzz}^{(2)}[(1-r)\langle\cos\theta\sin^2\theta\sin^2\phi\rangle + r\langle\cos\theta\rangle] \\ \chi_{YYZ}^{(2)} &= N\alpha_{zzz}^{(2)}[(1-r)\langle\cos\theta\sin^2\theta\cos^2\phi\rangle + r\langle\cos\theta\rangle] \\ \chi_{XZX}^{(2)} &= \chi_{ZXX}^{(2)} = N\alpha_{zzz}^{(2)}(1-r)\langle\cos\theta\sin^2\theta\sin^2\phi\rangle \\ \chi_{YZY}^{(2)} &= \chi_{ZYY}^{(2)} = N\alpha_{zzz}^{(2)}(1-r)\langle\cos\theta\sin^2\theta\cos^2\phi\rangle \\ \chi_{ZZZ}^{(2)} &= N\alpha_{zzz}^{(2)}[r\langle\cos\theta\rangle + (1-r)\langle\cos^3\theta\rangle]. \end{split}$$

As noted above, the XY-plane is defined in the laboratory coordinates system as the plane of the interface and the Z-axis is along the surface normal. N is the surface density of molecules, θ is the polar angle of the symmetry axis with respect to the Z axis, ϕ is the angle between the macroscopic X- and microscopic x-axes.

It is noted that all ϕ terms are averaged out due to the isotropic in-plane distribution $\langle \sin^2 \phi \rangle = \langle \cos^2 \phi \rangle = 1/2$. At equilibrium ($t = -\infty$), the surface susceptibilities can be simplified into the following:^{31,60}

$$\chi^{(2)}_{XXZ}(-\infty) = \chi^{(2)}_{YYZ}(-\infty) = \frac{1}{2}N\alpha^{(2)}_{zzz}[(1+r)\langle\cos\theta\,(-\infty)\rangle - (1-r)\langle\cos^3\theta\,(-\infty)\rangle]$$

(1)

PLEASE OTE THIS ARTIQLE AS DOI: 10.1063/5.0230223

$$\chi_{XZX}^{(2)}(-\infty) = \chi_{YZY}^{(2)}(-\infty) = \chi_{ZYY}^{(2)}(-\infty) = \chi_{ZXX}^{(2)}(-\infty)$$

$$= \frac{1}{2}N\alpha_{zzz}^{(2)}[(1-r)\langle\cos\theta(-\infty)\rangle - \langle\cos^{3}\theta(-\infty)\rangle]$$

$$\chi_{ZZZ}^{(2)}(-\infty) = N\alpha_{zzz}^{(2)}[r\langle\cos\theta(-\infty)\rangle + (1-r)\langle\cos^{3}\theta(-\infty)\rangle].$$
(2)

By choosing two linearly-polarized pulses, polarized parallel (X-axis) and perpendicular (Yaxis) to the incident plane, the probabilities, ρ_I , for the excitation of a molecule whose transition dipole moment is oriented with an out-of-plane angle, θ , and an in-plane angle, ϕ , are determined by⁶

$$\rho_X = |\mu \cdot E_X|^2 = |\mu|^2 |E_X|^2 \sin^2 \theta \cos^2 \phi$$

$$\rho_Y = |\mu \cdot E_Y|^2 = |\mu|^2 |E_Y|^2 \sin^2 \theta \sin^2 \phi.$$
(3)

Dipoles with a larger θ angle (more nearly in-plane) have a greater probability of excitation due to the $\sin^2 \theta$ term for both the X- and Y-polarized pumps. In the case of the X-polarized pump, dipoles with a smaller angle ϕ (lie more nearly along the X-axis) have a higher probability of being excited due to the $\cos^2 \phi$ term, while it is the opposite in the case of the Y-polarized pump. Upon excitation by a linearly-polarized pump, the symmetry of the interface with $C_{\infty V}$ is lifted and the symmetry of the in-plane distribution is no longer isotropic. The orientational distributions of dipoles excited by an X- or Y-polarized pump are depicted in Figures 1 (B) and (C), respectively. Thus, the time evolutions of orientational distribution for the non-equilibrium states are given by $\rho_g(t) = G(\Omega_t, t; \Omega_0, 0) \rho_{eq}(1 - \rho_I)$ and $\rho_e(t) = G(\Omega_t, t; \Omega_0, 0) \rho_{eq} \rho_I$ (I=X, Y),^{5, 6, 61-63} where ρ_g and ρ_e are the conditional probabilities of molecular orientation under perturbed ground and excited state conditions, respectively. Ω_0 and Ω_t are the azimuthal angles (θ and ϕ , respectively) at times zero and t, ρ_{eq} is the molecular equilibrium orientational distribution, and ρ_X or ρ_Y are the pumpinduced probability as described above. The evolution function G relates the initial state $(\Omega_0, 0)$ and the final state (Ω_t, t) .

More often than not, four effective susceptibilities for SFG experiments are measured, including SSP, PPP, SPS, and PSS. 9, 31, 64-66 The first letter denotes the polarization of the sum frequency, the second one denotes the polarization of the visible pulse, and the last denotes the polarization of the IR pulse: arranged in the order of increasing wavelength. The susceptibilities are related to the seven second order susceptibilities by local field factors, L_{ii} , as expressed by 31 ,

$$\chi_{SSP}^{(2)}(-\infty) = L_{XX}L_{XX}L_{ZZ}\sin\beta_{3}\,\chi_{XXZ}^{(2)}(-\infty)$$

$$\chi_{SPS}^{(2)}(-\infty) = L_{XX}L_{ZZ}L_{XX}\sin\beta_{2}\,\chi_{XZX}^{(2)}(-\infty)$$

$$\chi_{PSS}^{(2)}(-\infty) = L_{ZZ}L_{XX}L_{XX}\sin\beta_{1}\,\chi_{ZXX}^{(2)}(-\infty)$$

$$\chi_{PPP}^{(2)}(-\infty) = L_{ZZ}L_{ZZ}\sin\beta_{1}\sin\beta_{2}\sin\beta_{3}\,\chi_{ZZZ}^{(2)}(-\infty) + L_{ZZ}L_{YY}L_{YY}\sin\beta_{1}\cos\beta_{2}\cos\beta_{3}\,\chi_{ZYY}^{(2)}(-\infty)$$

$$-L_{YY}L_{ZZ}L_{YY}\cos\beta_{1}\sin\beta_{2}\cos\beta_{3}\,\chi_{YZY}^{(2)}(-\infty)$$

$$-L_{YY}L_{YY}L_{ZZ}\cos\beta_{1}\cos\beta_{2}\sin\beta_{3}\,\chi_{YYZ}^{(2)}(-\infty),$$
(4)

where β_i are the incident or reflection angles of ω_i beams with respect to the surface normal.

PLEASE CITE THIS ARTICLE AS DOI: 10.1063/5.0230223

- Fublishing Chemica

For simplicity, we define a new pre-factor L_{IJK} to denote the product of three local field factors $(L_{II}L_{JJ}L_{KK})$. For example, L_{XXZ} is used to represent the $L_{XX}L_{XX}L_{ZZ}$. Therefore, the time-dependent ground state susceptibility, $\chi_g^{(2)}(t)$, for PPP-polarized SFG measurement as an example, is given by the following expression:

$$\begin{split} \chi_{g,PPP}^{(2)}(t) &= L_{YYZ}\chi_{YYZ}^{(2)}(t) + L_{ZYY}\chi_{ZYY}^{(2)}(t) + L_{YZY}\chi_{YZY}^{(2)}(t) + L_{ZZZ}\chi_{ZZZ}^{(2)}(t) \\ &= L_{YYZ}\chi_{YYZ}^{(2)}(t) + (L_{ZYY} + L_{YZY})\chi_{ZYY}^{(2)}(t) + L_{ZZZ}\chi_{ZZZ}^{(2)}(t) \\ &= L_{YYZ}N\alpha_{g,ZZZ}^{(2)}\left[(1-r)\langle\cos\theta\sin^{2}\theta\cos^{2}\phi\rangle_{\rho_{g}(t)} + r\langle\cos\theta\rangle_{\rho_{g}(t)}\right] \\ &+ (L_{ZYY} + L_{YZY})N\alpha_{g,ZZZ}^{(2)}(1-r)\langle\cos\theta\sin^{2}\theta\cos^{2}\phi\rangle_{\rho_{g}(t)} \\ &+ L_{ZZZ}N\alpha_{g,ZZZ}^{(2)}\left[r\langle\cos\theta\rangle_{\rho_{g}(t)} + (1-r)\langle\cos^{3}\theta\rangle_{\rho_{g}(t)}\right]. \\ &= \chi_{g,PPP}^{(2)}(-\infty) - n(t)\alpha_{g,ZZZ}^{(2)}\left[C_{1,PPP}\langle\cos\theta\rangle_{t} + C_{2,PPP}\langle\cos\theta\sin^{2}\theta\cos^{2}\phi\rangle_{t} + C_{3,PPP}\langle\cos^{3}\theta\rangle_{t}\right]. \end{split}$$
 (5)

For simplicity, we define the following coefficients in Eq 5:

$$C_{1,PPP} = (L_{YYZ} + L_{ZZZ})r$$

 $C_{2,PPP} = (L_{YYZ} + L_{ZYY} + L_{YZY})(1-r)$
 $C_{3,PPP} = L_{ZZZ}(1-r)$

In the case of *X*-polarized photoexcitation, the time correlation functions in Eq 5 could be obtained with the similar derivation described above,

$$\begin{split} \langle\cos\theta\rangle_{t,X} &= \int d\Omega_t \int d\Omega_0 \cos\theta_t \, G(\Omega_t,t;\Omega_0,0) \rho_{eq}(\theta_0) \sin^2\theta_0 \cos^2\phi_0, \\ \langle\cos\theta\sin^2\theta\cos^2\phi\rangle_{t,X} &= \int d\Omega_t \int d\Omega_0 \cos\theta_t \sin^2\theta_t \cos^2\phi_t \, G(\Omega_t,t;\Omega_0,0) \rho_{eq}(\theta_0) \sin^2\theta_0 \cos^2\phi_0\,, \\ \text{and} \\ \langle\cos^3\theta\rangle_{t,X} &= \int d\Omega_t \int d\Omega_0 \cos^3\theta_t \, G(\Omega_t,t;\Omega_0,0) \rho_{eq}(\theta_0) \sin^2\theta_0 \cos^2\phi_0. \end{split}$$

With Eq 3, the expression of pumping probability functions, three correlation functions at a time *t* in Eq 5 under *Y*-polarized excitation with the evolution function *G* become

$$\begin{split} \langle\cos\theta\rangle_{t,Y} &= \int d\Omega_t \int d\Omega_0 \cos\theta_t \, G(\Omega_t,t;\Omega_0,0) \rho_{eq}(\theta_0) \sin^2\theta_0 \sin^2\phi_0, \\ \langle\cos\theta\sin^2\theta\cos^2\phi\rangle_{t,Y} &= \int d\Omega_t \int d\Omega_0 \cos\theta_t \sin^2\theta_t \cos^2\phi_t \, G(\Omega_t,t;\Omega_0,0) \rho_{eq}(\theta_0) \sin^2\theta_0 \sin^2\phi_0, \\ \text{and} \end{split}$$

$$\langle \cos^3 \theta \rangle_{t,Y} = \int d\Omega_t \int d\Omega_0 \cos^3 \theta_t \, G(\Omega_t, t; \Omega_0, 0) \rho_{eq}(\theta_0) \sin^2 \theta_0 \sin^2 \phi_0. \tag{7}$$

As we demonstrated in Eqs. 3, the polarization of the pump pulse results in different excitation

PLEASE OTE THIS ARTICLE AS DOI: 10.1063/5.0230223

polarized SFG measurement under excitation along the X or Y-axis have a similar form to the timedependent terms in Eq. 5, but with hyperpolarizabilities of the excited state:

$$\begin{split} \chi_{e,PPP}^{(2)}(t) &= L_{YYZ}\chi_{YYZ}^{(2)}(t) + L_{ZYY}\chi_{ZYY}^{(2)}(t) + L_{YZY}\chi_{YZY}^{(2)}(t) + L_{ZZZ}\chi_{ZZZ}^{(2)}(t) \\ &= L_{YYZ}\chi_{YYZ}^{(2)}(t) + (L_{ZYY} + L_{YZY})\chi_{ZYY}^{(2)}(t) + L_{ZZZ}\chi_{ZZZ}^{(2)}(t) \\ &= L_{YYZ}N\alpha_{e,ZZZ}^{(2)} \big[(1-r)\langle\cos\theta\sin^2\theta\cos^2\phi\rangle_{\rho_e(t)} + r\langle\cos\theta\rangle_{\rho_e(t)} \big] \\ &+ (L_{ZYY} + L_{YZY})N\alpha_{e,ZZZ}^{(2)}(1-r)\langle\cos\theta\sin^2\theta\cos^2\phi\rangle_{\rho_e(t)} \\ &+ L_{ZZZ}N\alpha_{e,ZZZ}^{(2)} \big[r\langle\cos\theta\rangle_{\rho_e(t)} + (1-r)\langle\cos^3\theta\rangle_{\rho_e(t)} \big] \\ &= n(t)\alpha_{e,ZZZ}^{(2)} \big[C_{1,PPP}\langle\cos\theta\rangle_t + C_{2,PPP}\langle\cos\theta\sin^2\theta\cos^2\phi\rangle_t + C_{3,PPP}\langle\cos^3\theta\rangle_t \big] \end{split}$$
 (8)

We can then simplify this expression by combining coefficients and plugging in Eq. 5 such that

$$\chi_{e,PPP}^{(2)}(t) = \frac{\alpha_{e,zzz}^{(2)}}{\alpha_{g,zzz}^{(2)}} \left(\chi_{g,PPP}^{(2)}(-\infty) - \chi_{g,PPP}^{(2)}(t) \right), \tag{9}$$

and find that the time-dependent excited stated susceptibility when pumped along the X or Y-axis is the product of the excited and ground state hyperpolarizability ratio and the difference between the equilibrium and time-dependent ground state susceptibilities.

By combining Eq 5 and Eq 8, the total time-dependent susceptibilities for and PPP- SFG measurements under X-polarized pump are

$$\begin{split} \chi_{total,PPP,X}^{(2)}(t) &= \chi_{g,PPP,X}^{(2)}(t) + \chi_{e,PPP,X}^{(2)}(t) \\ &= \chi_{g,PPP,X}^{(2)}(-\infty) \\ &\qquad \qquad - n(t) \left(\alpha_{g,zzz}^{(2)} - \alpha_{e,zzz}^{(2)} \right) \left[C_{1,PPP} \langle \cos \theta \rangle_{t,X} \\ &\qquad \qquad + C_{2,PPP} \langle \cos \theta \sin^2 \theta \cos^2 \phi \rangle_{t,X} + C_{3,PPP} \langle \cos^3 \theta \rangle_{t,X} \right] \\ &= \chi_{g,PPP,X}^{(2)}(-\infty) \\ &\qquad \qquad - n(t) \Delta \alpha_{ge,zzz}^{(2)} \left[C_{1,PPP} \langle \cos \theta \rangle_{t,X} + C_{2,PPP} \langle \cos \theta \sin^2 \theta \cos^2 \phi \rangle_{t,X} \\ &\qquad \qquad + C_{3,PPP} \langle \cos^3 \theta \rangle_{t,X} \right] \end{split}$$
(10)

Likewise, the total time-dependent susceptibilities for PPP-SFG measurements under Ypolarized pump are

PLEASE OTE THIS ARTIQLE AS DOI: 10.1063/5.0230223

 $\chi^{(2)}_{total,PPP,Y}(t) = \chi^{(2)}_{g,PPP,Y}(t) + \chi^{(2)}_{e,PPP,Y}(t)$ $=\chi_{g,PPP,Y}^{(2)}(-\infty)$ $- \, n(t) \Delta \alpha_{ge,zzz}^{(2)} \big[\mathcal{C}_{1,PPP} \langle \cos\theta \rangle_{t,Y} + \mathcal{C}_{2,PPP} \langle \cos\theta \sin^2\theta \cos^2\phi \rangle_{t,Y} \\$ + $C_{3,PPP}\langle \cos^3\theta\rangle_{t,Y}$]. (11)

Generally, these expressions show that the time dependent susceptibility is equal to the difference between the total time-dependent and equilibrium susceptibilities as well as the difference between the total time-dependent and ground state susceptibilities: $\Delta \chi^{(2)}(t) = \chi^{(2)}_{total}(t) - \chi^{(2)}_{total}(-\infty) =$ $\chi_{total}^{(2)}(t) - \chi_{q}^{(2)}(-\infty).$

Experimentally, the changes in susceptibility over time, $\Delta \chi^{(2)}_{total,PPP}(t)$, is measured, and equals the difference between the total and ground state susceptibilities. By subtracting Eq. 5 from Eqs. 10 or 11 we find

$$\begin{split} \Delta\chi_{total,PPP,X}^{(2)}(t) &= -n(t)\Delta\alpha_{ge,zzz}^{(2)} \left[C_{1,PPP} \langle \cos\theta \rangle_{t,X} + C_{2,PPP} \langle \cos\theta \sin^2\theta \cos^2\phi \rangle_{t,X} \right. \\ &\quad + C_{3,PPP} \langle \cos^3\theta \rangle_{t,X} \right] \\ \Delta\chi_{total,PPP,Y}^{(2)}(t) &= -n(t)\Delta\alpha_{ge,zzz}^{(2)} \left[C_{1,PPP} \langle \cos\theta \rangle_{t,Y} + C_{2,PPP} \langle \cos\theta \sin^2\theta \cos^2\phi \rangle_{t,Y} \right. \\ &\quad + C_{3,PPP} \langle \cos^3\theta \rangle_{t,Y} \right]. \end{split} \label{eq:delta_total_PPP} \tag{12}$$

The X- and Y-polarized linear pump pulses induce the same out-of-plane orientations of θ but the different in-plane motions of ϕ . Then the sum of the change of susceptibilities induced by Xand Y-polarized pump pulses gives the out-of-plane dynamics. To isolate in-plane orientational dynamics from out-of-plane orientational dynamics, we simply subtract $\Delta \chi^{(2)}$ for X- and Ypolarized photoexcitations, the out-of-plane terms could be combined or canceled out in the simplification

$$\begin{split} \Delta\chi_{PPP,X-Y}^{(2)}(t) &= \Delta\chi_{total,PPP,X}^{(2)}(t) - \Delta\chi_{total,PPP,Y}^{(2)}(t) \\ &= -n(t)\Delta\alpha_{ge,zzz}^{(2)}C_{2,PPP}(\langle\cos\theta\sin^2\theta\cos^2\phi\rangle_{t,X} - \langle\cos\theta\sin^2\theta\cos^2\phi\rangle_{t,Y}) \\ &= -n(t)\Delta\alpha_{ge,zzz}^{(2)}C_{2,PPP}\langle\cos\theta\sin^2\theta\rangle_{t} \big[\langle\cos^2\phi\rangle_{t,X} - \langle\cos^2\phi\rangle_{t,Y}\big] \\ &= -n(t)\Delta\alpha_{ge,zzz}^{(2)}C_{2,PPP}\langle\cos\theta\sin^2\theta\rangle_{t} \Big[2\langle\cos^2\phi\rangle_{t,X-Y} - \frac{1}{2}\Big] \end{split}$$

$$(13)$$

with $\langle \cos \theta \rangle_{t,X} = \langle \cos \theta \rangle_{t,Y}$ and $\langle \cos^3 \theta \rangle_{t,X} = \langle \cos^3 \theta \rangle_{t,Y}$. Additionally, the $\langle \cos \theta \sin^2 \theta \rangle_t$ term was able to be factored out because they are the same for both X- and Y-polarized pump excitation.

Eq 13 shows that the time-resolved PPP- SFG measurements are related to time-dependent population evolution, n(t), time-dependent out-of-plane dynamics, $\langle \cos \theta \sin^2 \theta \rangle_t$, and timedependent in-plane dynamics, $2\langle \cos^2 \phi \rangle_{t,X-Y}$. The population dynamics occur on the order of tens of nanoseconds, 62 and are not considered here. Knowing $\langle \cos\theta \sin^2\theta \rangle_t$ from the out-of-plane experiments, 67 we can obtain the time-dependent in-plane orientational time constant, τ_{ϕ} , based on the assumption that out-of-plane and in-plane time evolutions are uncoupled, namely,

PLEASE OTE THIS ARTICLE AS DOI: 10.1063/5.0230223

If we assume that the out-of-plane term in Eq. 13, $\langle \cos \theta \sin^2 \theta \rangle_t$, happens on a time scale much longer than in in-plane term, $\left[2\langle\cos^2\phi\rangle_{t,X-Y}-\frac{1}{2}\right]$, we can then omit the out-of-plane contributions and substitute Eq. 14 into Eq. 13. The change in the difference of the X- and Y-polarized susceptibilities, $\Delta \chi_{PPP,X-Y}^{(2)}(t)$, can then be fit with a single exponential fitting and thereby extract the relaxation time constants for the inplane dynamics of a given functional group.

Experimental section

The details of our TR-VSFG experimental setup have been described previously.^{5, 44} Briefly, an IR beam with a typical energy of 1.5 µJ per pulse was focused onto the sample by a BaF₂ lens with a 100 mm focal length at 67° relative to the surface normal and a spot size of around 120 µm in diameter. A picosecond 400 nm pulse with a width of 10 ps and a pulse energy of 8 µJ was focused to a 210 µm spot size by a BaF₂ lens of a 250 mm focal length at 76° relative to the surface normal. A 409 nm pump pulse with a pulse energy of 5 µJ (<100 fs) was focused on the sample from the top by a BaF₂ lens of a 500 mm focal length along the surface normal with a focal spot of 800 µm, as schematically shown in Figure 1 (A). The polarization of the X- and Y- polarized pump beam was controlled using a zero-order half-wave plate. The generated SFG signal, which propagates with an angle along the X-axis, was focused into a monochromator and detected by a photomultiplier tube (PMT) (Hamamatsu) when the time-profile experiments were performed. The SFG signals from PMT were sent into a lock-in amplifier with reference to a 500 Hz chopper frequency in the pump arm, which was followed by a Boxcar gating averager. A translational stage and the SFG signal sampling from the lock-in amplifier were controlled by a computer using LabVIEW. The polarizations of the SFG pulses are defined as S or P: perpendicular or parallel to the incident plane, respectively, and are listed in order of increasing wavelength: SFG signal, visible, IR.

Results and Discussion

To investigate in-plane orientational dynamics of interfacial molecules, we made PPPpolarized SFG measurements of the -C=O and -CF₃ groups of C153 with resonances centered at 1718 cm⁻¹ and 1319 cm⁻¹, respectively.⁶⁷ Figure 2(A) shows the time traces of the PPP-polarized SFG electric fields for the -C=O group under both X- and Y-polarized excitation. The amplitude of the electric field is the square root of the intensity. All time-dependent SFG electric fields were normalized with the SFG electric field without pumping (at t<0) to account for contributions from ground state molecules. The initial decrease in the SFG electric field is attributed to the ground state bleaching of C153 and cancelations due to a phase difference of π between ground state and

This is the author's peer reviewed, accepted manuscript. However, the online version of record will be different from this version once it has been copyedited and typeset PLEASE CITE THIS ARTICLE AS DOI: 10.1063/5.0230223

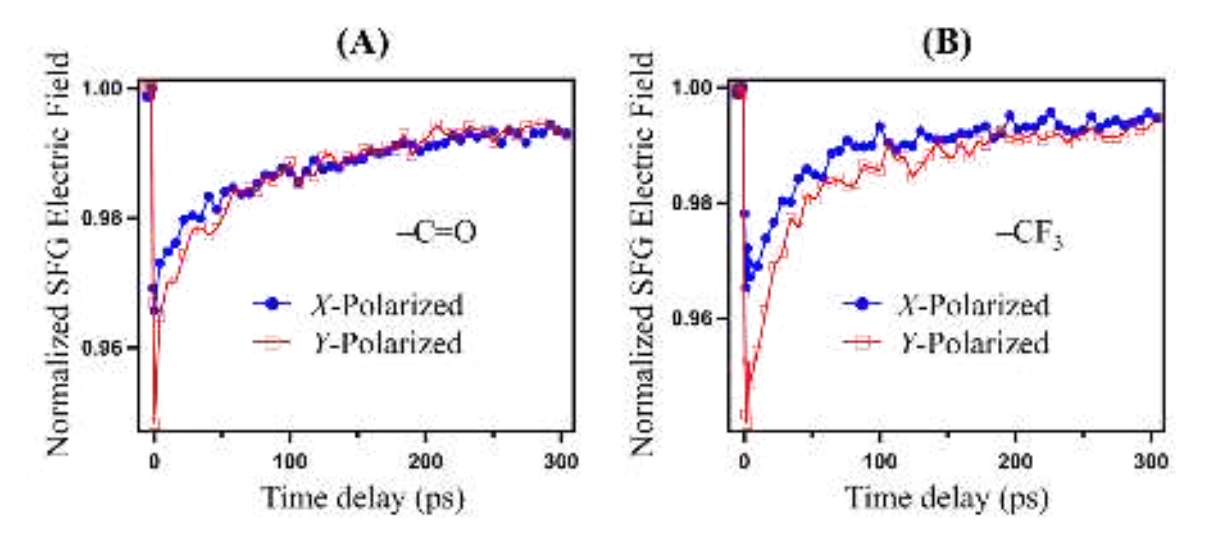


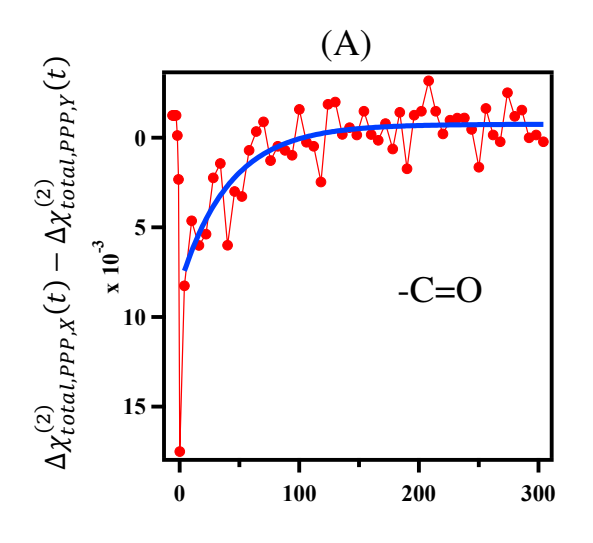
Figure 2. Time traces of PPP SFG electric fields under X- and Y- polarized pump. (A) -C=O group; (B) $-CF_3$ group.

the newly excited state molecules in such a two-level system.^{6, 7} Under Y-polarized excitation, a decrease in SFG electric field is also seen at initial time t=0 relative to the X-polarized data, which is due to the different sensitivity of the PPP-polarized hyperpolarizabilities to the X- and Ypolarized excitation. Over time, the SFG recovery curves reach the same signal level when an orientational equilibrium is reached and in-plane isotropy is reestablished, on the order of ~70 ps. This indicates that the same equilibrium orientational distribution is reached regardless of the initial excitation due to pump polarization. We then conducted the same experiments, probing the— CF₃ group, as shown in Figure 2(B). Here, it is shown that at t=0, there is an even greater difference in the initial intensities based on pump polarization than for the -C=O group, since the two functional groups have different polarizability responses to the photoexcitation. For the -CF₃ group, we see that the SFG responses for the two differently polarized pumps also equilibrate and continue to increase parallel to each other, but only take about 140 ps. As described in Eq. 12, we can isolate in-plane motions of interfacial molecules from their out-of-plane counterparts using the TR-VSFG signals under two linearly-polarized pump pulses. Figures 3(A) and 3(B) show the timedependent difference in the SFG electric fields under X- and Y-polarized pump for the -C=O and -CF₃ groups, respectively. It is interesting to note that the positive signature of the difference for both the pumps suggest the magnitude for $\alpha_{g,zzz}^{(2)}$ is less than that for $\alpha_{e,zzz}^{(2)}$. The time traces of the SFG electric fields for the two groups were fitted to a single-exponential plus baseline, giving the in-plane rotational time constants of $\mu_{-C=0}$ and μ_{-CF_3} to be 41.5 ± 8.2 ps and 36.0 ± 4.5 ps, respectively. Due to the large relative error of the time constants, we cannot say with certainty that the functional groups behave very differently over time in the interfacial plane. With improved experimental signal-to-noise ratios and more specialized instrumentation, such as difference, or lack thereof, can likely be solidified. Nevertheless, these specific in-plane dynamics of functional groups are still important and may differ from the out-of-plane process.

The in-plane rotational time constants indicate that the rotational motions for the two groups are slower at the interfacial plane than that in bulk. In bulk acetonitrile, the -C=O group of a structurally similar molecule, coumarin 314 has a rotational time of around 26 ± 2 ps, 68 faster than

PLEASE OTE THIS ARTIQLE AS DOI: 10.1063/5.0230223

the air/water interface. Owing to the high solvent-solute collision rate, the solute rotational motion is significantly hindered, and can be viewed as a succession of very small angle rotation around a randomly oriented axis.⁶⁹ Therefore, the property of the in-plane rotation of the two functional groups is likely to be resistant at the air/water interface.



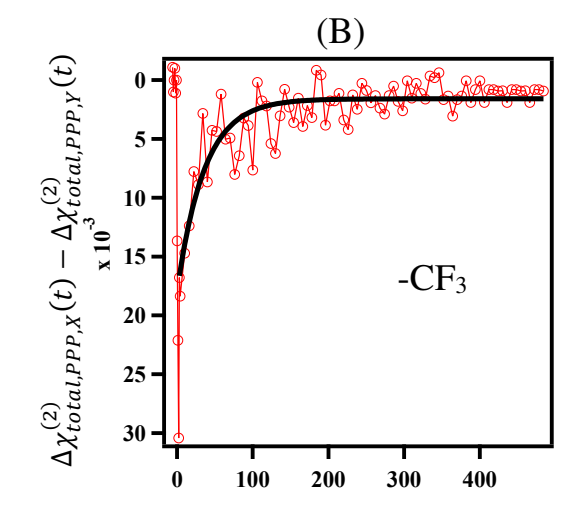


Figure 3. The time-dependent difference in SFG electric fields under the X- and Ypolarized pump for the -C=O (A) and -CF₃ (B) groups. The solid line is a fit to a single exponential plus baseline yields the in-plane rotational time constants of $\mu_{-C=0}$ and $\mu_{\rm -CF_2}$ to be 41.5 ± 8.2 ps and 36.0 ± 4.5 ps, separately.

Previous TR-SHG studies showed that the time evolution of in-plane rotations of the permanent dipole of C153 exhibit a rotational time of 198 ± 15 ps, 70 which is five times faster than those for the -C=O and -CF₃ groups found here. It is not surprising that the SHG and SFG methods yield strikingly different values for the in-plane rotation since they probe different moieties of the molecule. According to the geometric dimension, the size of the permanent dipole of C153 (6.10 Å) is almost five times those of the -C=O and -CF₃ groups (1.20 Å and 1.34 Å).⁶⁹ Other studies have been carried out on molecular rotational dynamics at liquid interfaces by measuring the decay in the fluorescence anisotropy of interfacial molecules. 71-73 The rates of in-plane motions for the – C=O and -CF3 groups are significantly different from their out-of-plane counterparts, which exhibited distinct orientational angle change over time.⁶⁷ As shown in the companion article, the orientational angle for the -C=O group immersed in water changes by 4°, followed by an orientational recovery time of 130 ± 20 ps upon excitation. On the other hand, the -CF₃ group in the air exhibits a change in orientational angle of 8° with a much slower orientational recovery time of 210 ± 38 ps. ⁶⁷ Distinct from those for the out-of-plane motions, the time progression of the -C=O group motions for the in-plane motion is slower than that for the -CF₃ group. It seems that the out-of-plane motions are related to the motion of the whole molecule while the in-plane motions are more localized. The -C=O and -CF₃ groups possess different properties in terms of size, shape, charge distribution such as dipole moment and polarizability, polarity, and hydrogen bonding. As schematically shown in Figure 4, the more polar nature of -C=O group immersed on the water side, being both highly charged and solvent accessible, is likely to cause hydrogen bonding and dielectric friction. On the other hand, the hydrophobic -CF₃ group on the air side

PLEASE OTE THIS ARTIQLE AS DOI: 10.1063/5.0230223

experiences pure mechanical friction in the highly nonpolar interfacial environment.

On the theoretical side, Benjamin et al. have examined the rotational anisotropy of interfacial solutes using two different correlation functions for in-plane and out-of-plane motions,^{74, 75} and found that no significant difference between in-plane and out-of-plane motions for a low dipole moment solute was observed.⁷⁴ However, molecular dynamics simulations on coumarin 314 showed that the in-plane rotation is characterized by a sequence of diffusive-like steps interrupted by flipping episodes, whereas out-of-plane motions include large-amplitude oscillations modulated by small-amplitude oscillations.⁷⁶ Our findings provide strong evidence that different moieties of interfacial molecules can manifest a significant difference between in-plane and out-of-plane motion, originating from local frictions from different directions on the differing moieties. While the concept of interfacial solvent friction has been rarely used to quantitatively rationalize solute-solvent interactions, a more systematic and quantitative investigation of this important concept requires more theoretical studies and experimental data.

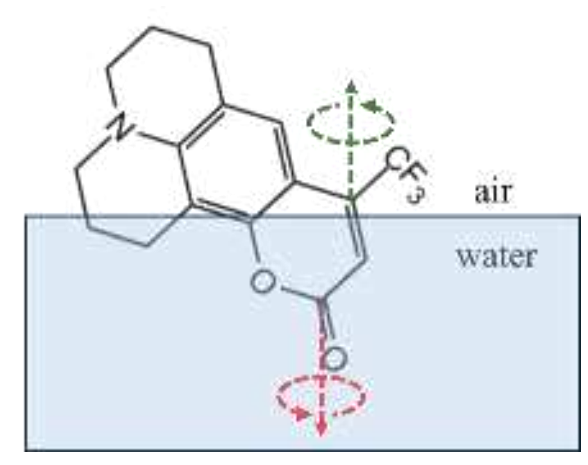


Figure 4. Schematic depiction of in-plane functional group rotation for the –C=O and – CF₃ groups of Coumarin 153 at the air/water interface.

Conclusions

We have presented the in-plane rotational dynamics of the vibrational probes for the -C=O and $-CF_3$ groups of coumarin 153 (C153) at the air/water interface by using femtosecond time-resolved vibrational sum frequency spectroscopy. The in-plane orientational time constants of the -C=O and $-CF_3$ groups of C153 are found to be 41.5 ± 8.2 ps and 36.0 ± 4.5 ps, respectively. The findings suggest that the in-plane dynamics of the individual functional groups progress on timescales five-times faster than the molecule as a whole. While no significant difference can be drawn between the dynamics of the -C=O and $-CF_3$ groups of C153, our TR-SFG experiments provided their direct quantification for the first time. The difference in orientational motion reveals the microscopic heterogeneity where C153 molecules are located at the interface. Further improvements of the experimental systems will likely provide certainty of the relationships between the dynamics experienced by functional groups of the same molecule which do not share the same solvent conditions. These structural dynamics for molecular moieties have implications in molecular rotations, energy transfer, and charge transfer at biological cell/membrane and aqueous interfaces.

accepted manuscript. However, the online version of record will be different from this PLEASE QITE THIS ARTICLE AS DOI: 10.1063/5.0230223

Acknowledgment

This project was initiated at Columbia University and finished at Utah State University. Y.R. expressed his great gratitude to Drs. Kenneth B. Eisenthal and Nicholas J. Turro for their mentorships. This material is based upon work supported by the National Science Foundation under Grant No. [2045084].

#Those authors contributed equally to this work.

References

- ¹N. K. Adam, *The Physics and Chemistry of Surfaces* (Oxford University Press, London, 1991),
- ² A. W. Adamson, and A. P. Gast, *Physical chemistry of surfaces* (New York: Wiley, New York, 1997).
- ³ D. K. Chattoraj, Adsorption and the Gibbs surface excess (Plenum Press, New York, 1984),
- ⁴M. F. Ruiz-Lopez *et al.*, Nat. Rev. Chem. **4** (2020) 459.
- ⁵ Y. Rao *et al.*, J. Phys. Chem. B **112** (2008) 13572.
- ⁶D. Zimdars *et al.*, J. Phys. Chem. B **103** (1999) 3425.
- ⁷ Y. Rao *et al.*, J. Phys. Chem. C **115** (2011) 11678.
- ⁸ X. M. Shang *et al.*, J. Phys. Chem. C **112** (2008) 20375.
- ⁹P. B. Miranda, and Y. R. Shen, J. Phys. Chem. B **103** (1999) 3292.
- ¹⁰ K. B. Eisenthal, Chem. Rev. **96** (1996) 1343.
- ¹¹G. L. Richmond, Chem. Rev. **102** (2002) 2693.
- ¹² M. Mucha *et al.*, J. Phys. Chem. B **109** (2005) 7617.
- ¹³ Y. R. Shen, *The Principles of Nonlinear Optics* (John Wiley & Sons, Inc, Hoboken, New Jersey, 2003),
- ¹⁴ Y. R. Shen, Annu. Rev. Phys. Chem. **40** (1989) 327.
- ¹⁵ Y. R. Shen, IEEE J. Sel. Top. Quantum Electron. **6** (2000) 1375.
- ¹⁶ T. F. Heinz, H. W. K. Tom, and Y. R. Shen, Phys. Rev. A **28** (1983) 1883.
- ¹⁷ A. Castro, K. Bhattacharyya, and K. B. Eisenthal, J. Chem. Phys. **95** (1991) 1310.
- ¹⁸ Y. Rao, N. J. Turro, and K. B. Eisenthal, J. Phys. Chem. C **113** (2009) 14384.
- ¹⁹ D. Zhang, J. H. Gutow, and K. B. Eisenthal, Journal of the Chemical Society-Faraday Transactions **92** (1996) 539.
- ²⁰G. L. Richmond, Annu. Rev. Phys. Chem. **52** (2001) 357.
- ²¹G. Ma, and H. C. Allen, Langmuir **22** (2006) 5341.
- ²² M. J. Shultz *et al.*, Int. Rev. Phys. Chem. **19** (2000) 123.
- ²³ S. Baldelli, M. Mascal, and J. C. Bertran, Chem. Phys. Lett. **427** (2006) 72.
- ²⁴ S. Z. Can *et al.*, J. Phys. Chem. C **111** (2007) 8739.
- ²⁵ F. Ding *et al.*, J. Phys. Chem. C **114** (2010) 17651.
- ²⁶ J. T. Fourkas *et al.*, J. Phys. Chem. C **111** (2007) 8902.
- ²⁷ F. M. Geiger, Annu. Rev. Phys. Chem. **60** (2009) 61.
- ²⁸ J. Wang, S. H. Lee, and Z. Chen, J. Phys. Chem. B **112** (2008) 2281.
- ²⁹ J. Liu, and J. C. Conboy, J. Am. Chem. Soc. **126** (2004) 8894.
- ³⁰ X. Chen, L. B. Sagle, and P. S. Cremer, J. Am. Chem. Soc. **129** (2007) 15104.
- ³¹ H.-F. Wang *et al.*, Int. Rev. Phys. Chem. **24** (2005) 191.
- ³² R. Lu *et al.*, J. Phys. Chem. B **108** (2004) 7297.
- ³³ A. N. Bordenyuk, and A. V. Benderskii, J. Chem. Phys. **122** (2005)
- ³⁴G. Ma *et al.*, Appl. Spectrosc. **63** (2009) 528.
- ³⁵ E. V. Sitzmann, and K. B. Eisenthal, J. Phys. Chem. **92** (1988) 4579.

accepted manuscript. However, the online version of record will be different from this

PLEASE CITE THIS ARTICLE AS DOI: 10.1063/5.0230223

- ³⁶ K. Sekiguchi, S. Yamaguchi, and T. Tahara, J. Chem. Phys. **128** (2008) 114715.
- ³⁷ A. L. Harris, and L. Rothberg, J. Chem. Phys. **94** (1991) 2449.
- ³⁸ J. A. McGuire, and Y. R. Shen, Science **313** (2006) 1945.
- ³⁹ M. Smits *et al.*, Phys. Rev. Lett. **98** (2007) 098302.
- ⁴⁰ A. Ghosh *et al.*, Rev. Sci. Instrum. **79** (2008) 093907.
- ⁴¹ E. H. G. Backus *et al.*, Science **310** (2005) 1790.
- ⁴² Z. Wang *et al.*, Science **317** (2007) 787.
- ⁴³ Y. Rao *et al.*, J. Phys. Chem. B **112** (2008) 13572.
- ⁴⁴ Y. Rao, N. J. Turro, and K. B. Eisenthal, J. Phys. Chem. C **114** (2010) 17703.
- ⁴⁵ S. Nihonyanagi *et al.*, Bull. Chem. Soc. Jpn. **85** (2012) 758.
- ⁴⁶ B. Xiang *et al.*, Sci. Adv. **3** (2017) e1701508.
- ⁴⁷ G.-H. Deng *et al.*, Proc. Natl. Acad. Sci. U.S.A. **118** (2021) e2100608118.
- ⁴⁸ Z. C. Huang-Fu et al., JACS Au **3** (2023) 1413.
- ⁴⁹ Z. C. Huang-Fu *et al.*, ACS Phys Chem Au **3** (2023) 374.
- ⁵⁰ C.-S. Hsieh *et al.*, Phys. Rev. Lett. **107** (2011) 116102.
- ⁵¹ H.-K. Nienhuys, and M. Bonn, J. Phys. Chem. B **113** (2009) 7564.
- ⁵² M. Bonn, Y. Nagata, and E. H. G. Backus, Angew. Chem. Int. Ed. **54** (2015) 5560.
- ⁵³ S. Malyk *et al.*, J. Phys. Chem. C **117** (2013) 935.
- ⁵⁴D. Bhattacharyya *et al.*, J. Phys. Chem. Lett. **10** (2019) 5434.
- ⁵⁵ J. Ho *et al.*, J. Phys. Chem. C **120** (2016) 12578.
- ⁵⁶ K. T. Nguyen, X. M. Shang, and K. B. Eisenthal, J. Phys. Chem. B **110** (2006) 19788.
- ⁵⁷ C. Hirose, N. Akamatsu, and K. Domen, Appl. Spectrosc. **46** (1992) 1051.
- ⁵⁸ C. Hirose, N. Akamatsu, and K. Domen, J. Chem. Phys. **96** (1992) 997.
- ⁵⁹ D. Zhang *et al.*, J. Chem. Phys. **98** (1993) 5099.
- ⁶⁰ X. Zhuang et al., Phys. Rev. B **59** (1999) 12632.
- ⁶¹ T. J. Chuang, and K. B. Eisenthal, J. Chem. Phys. **57** (1972) 5094.
- ⁶² Z. Gengeliczki, D. E. Rosenfeld, and M. D. Fayer, J Chem Phys **132** (2010) 244703.
- ⁶³ H. K. Nienhuys, and M. Bonn, J. Phys. Chem. B **113** (2009) 7564.
- ⁶⁴ X. Wei et al., Phys. Rev. E **62** (2000) 5160.
- ⁶⁵ W. Gan et al., J. Phys. Chem. C **111** (2007) 8716.
- ⁶⁶ Y. Rao, M. Comstock, and K. B. Eisenthal, J. Phys. Chem. B **110** (2006) 1727.
- ⁶⁷ Y. Rao *et al.*, J. Chem. Phys. **150** (2019) 094709.
- ⁶⁸ M. Theisen *et al.*, J. Chem. Phys. **131** (2009)
- ⁶⁹ M. L. Horng, J. A. Gardecki, and M. Maroncelli, J. Phys. Chem. A **101** (1997) 1030.
- ⁷⁰ E. A. McArthur, Ph.D. dissertation, Columbia University (New York), 2008.
- ⁷¹ D. A. Piasecki, and M. J. Wirth, J. Phys. Chem. **97** (1993) 7700.
- ⁷² M. J. Wirth, and J. D. Burbage, Anal. Chem. **63** (1991) 1311.
- ⁷³ M. J. Wirth, and J. D. Burbage, J. Phys. Chem. **96** (1992) 9022.
- ⁷⁴ I. Benjamin, J. Chem. Phys. **127** (2007) 204712.
- ⁷⁵ I. Benjamin, Chem. Phys. Lett. **469** (2009) 229.
- ⁷⁶ D. A. Pantano, and D. Laria, J. Phys. Chem. B **107** (2003) 2971.